ACS APPLIED MATERIALS & INTERFACES

Research Article

www.acsami.org

Nonvolatile Organic Thin Film Transistor Memory Devices Based on Hybrid Nanocomposites of Semiconducting Polymers: Gold Nanoparticles

Hsuan-Chun Chang,[†] Cheng-Liang Liu,*[,‡] and Wen-Chang Chen*[,†]

[†]Department of Chemical Engineering, National Taiwan University, Taipei, 10617 Taiwan

[‡]Department of Chemical and Materials Engineering, National Central University, Taoyuan, 32001 Taiwan

Supporting Information

ABSTRACT: We report the facile fabrication and characteristics of organic thin film transistor (OTFT)-based nonvolatile memory devices using the hybrid nanocomposites of semiconducting poly(9,9-dioctylfluorene-alt-bithiophene) (F8T2) and ligand-capped Au nanoparticles (NPs), thereby serving as a charge storage medium. Electrical bias sweep/excitation effectively modulates the current response of hybrid memory devices through the charge transfer between F8T2 channel and functionalized Au NPs trapping sites. The electrical performance of the hybrid memory devices can be effectively controlled though the loading concentrations (0−9 %) of Au NPs and organic thiolate ligands on Au NP surfaces with different carbon chain lengths (Au-L6, Au-L10, and Au-L18). The memory window induced by voltage sweep is considerably increased by the high content of Au NPs or short carbon chain on the ligand. The hybrid nanocomposite of F8T2:9% Au-L6 provides the OTFT memories with a memory window of ∼41 V operated at ±30 V and memory ratio of $\sim 1 \times 10^3$ maintained for 1×10^4 s. The experimental results suggest that the hybrid materials of the functionalized Au NPs in F8T2 matrix have the potential applications for low voltage-driven high performance nonvolatile memory devices.

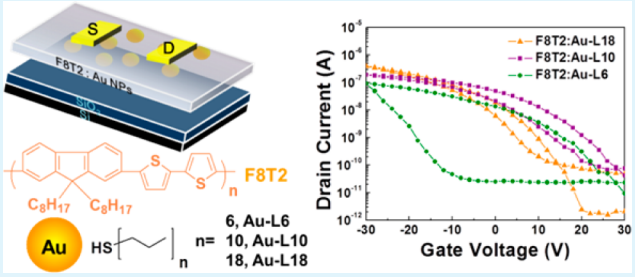

KEYWORDS: *nanocomposites, nonvolatile memory, gold nanoparticles, semiconducting polymer, transistor*

INTRODUCTION

Functional organic thin film transistors (OTFTs) have attracted extensive research efforts in recent years because of their tremendous emerging applications for flexible electronics.[1−5] Especially, OTFTs can serve as the basic and reliable media for electrical memories and switching devices in the increasingly important information technology. OTFTs with nonvolatile memory effects are one potential option based on their nondestructive readout and single transistor architectural compatibility for easily integrated devices.[5−10] Until now, three strategies have been used for OTFTs memory: (1) ferroelectric,[11] (2) polymer electret,[12−19] and (3) floating gates.[20−38] Both methods 1 and 2 are typical chargeable dielectrics from switchable dipole polarization and electric charge, respectively, whereas method 3 introduces charge traps into the gate dielectric. Device channel conductance can be modulated through the external dc voltage sweep/pulse bias, characterized by threshold voltage shift (ΔV_{th}, memory window) in a hysteresis of the OTFTs transfer curve or bi-(or multi-)stabilities as different drain current (I_d) states at a fixed gate voltage.

OTFTs with floating gate architecture can tune the threshold voltage over a wide range where the charges are stored in the floating gate. However, it meets the challenging problems on high power consumption and selection of suitable key materials for reproducibility even though the reversible mass storage is efficiently manipulated by charging or discharging a floating gate electrode.[5−10] Among all, metallic nanoparticles (NPs) were isolated through the blocking oxide/tunneling oxide[20−29] or chemically assembled inside the nanostructured block copolymers template,[30−33] acting as the floating gate of charge trapping centers and manipulating charge transport in OTFTs memory devices. Controllable trapping density and distribution through the synthesis of NPs coated with functional ligands were achieved for nanoscale high-density data storage to solve the scaling down problem.[30−35] Besides, fabrication of hybrid nanocomposites with charge-controlling guest materials proved to be demonstrated as significantly improved memory devices.[39−50] Therefore, simplified fabrication based on directly incorporating the metal NPs within organic semiconductors resulted in the variable and controllable electrical behaviors of OTFTs for reducing the power dissipation.[34−37] Previous reports such as ligand-modified NPs implanted at the bottom of organic semiconductor layer[34,35] or sandwiched structure by

Received: September 25, 2013
Accepted: November 13, 2013
Published: November 13, 2013

placing the thermally deposited NPs in between two semiconductor layers[36,37] provided the solutions to simultaneously make high density memory devices. In addition, polymer hybrid nanocomposites provided the stable electronic properties of inorganic components and structural flexibility of organic components for fulfilling resistance switching behavior.[48−50] Therefore, simple hybrids between polymer semiconductors and discrete functionalized inorganic Au NPs can be directly applied as channels/trapping centers of OTFTs device to fulfill the memory functionality without requirement on additional power consumption.[38] Our recent work based on electronspun P3HT:Au NPs nanofibers as semiconducting channel also showed the charge being stored or erased by applying appropriate gate voltage (3.5−10.6 V threshold voltage shifting within operation voltage of ±5 V).[51] Indeed, the presence of NP guests in the semiconducting polymer host matrix dramatically influences the OTFT memory device characteristics. Therefore, the variations on interparticle distances through the NP concentration and modified ligands on core NP surfaces play an important role in hybrid thin film morphology and its device performance.

In this work, we report the fabrication and characterization of nonvolatile OTFTs memory directly using hybrid thin films of F8T2 and ligand-capped Au NPs as the OTFTs channels. The simple interfacial ligand exchange method[52,53] was employed to prepare the Au NPs cationically substituted with thiol-protected ligands (Au-L6, Au-L10 and Au-L18) starting from oleyamine-stabilized Au NPs (Au-oley). The structures of modified Au NPs are shown in Figure 1. The p-type F8T2:Au NPs hybrid

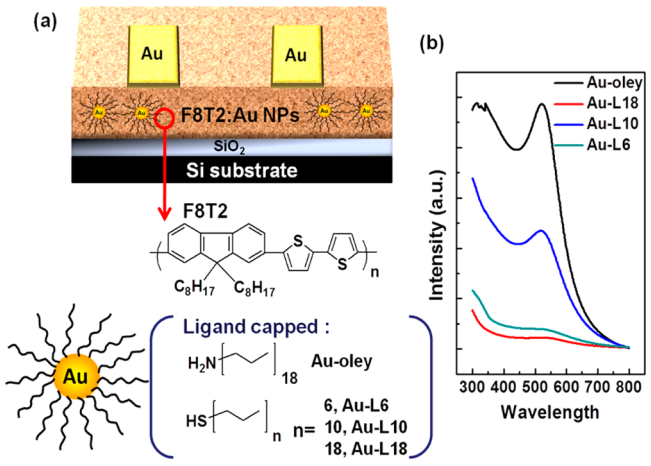

Figure 1. (a) Schematic configuration of the OTFTs memory devices on the SAM-modified SiO_2 surface using the hybrid materials of F8T2:ligand-capped Au NPs. (b) Optical absorption spectra of the modified-Au NPs.

nanocomposites were simply spin-coated on self-assembled monolayer (SAM) modified SiO_2 dielectric and viewed as the combined functionalities of the active current channel and the charge storage layer. The current hysteresis would be arisen from the charge trapping/detrapping interface between semiconducting F8T2/functionalized NPs during the voltage sweep. The effects of Au NPs content and alkylthiols chain length on the memory effects are explored. The experimental results suggested that high performance nonvolatile memory devices could be produced using the hybrid nanocomposites through the optimization on the Au composition and ligand carbon chain length.

EXPERIMENTAL SECTION

Materials. All commercially available reagents or anhydrous solvents obtained from suppliers were used without further purification unless otherwise noted. All the reagents and anhydrous solvents were purchased from Aldrich (USA). P-type semiconducting polymer, poly(9,9-dioctylfluorene-alt-bithiophene) (F8T2), was delivered from American Dye Source (Canada) (weight average molecular weight = 38 000 g mol^{-1}).

Synthesis of Oleyamine-Stabilized Au NPs (Au-oley). Synthesis of Au-oley was carried out as mentioned before.[52,53] A stirred solution of auric acid ($HAuCl_4 \cdot 3H_2O$; 1 mmol) and oleylamine (10 mmol) in 50 mL of toluene were added into a flask at 65 °C under a nitrogen atmosphere, kept at this temperature for 6 h and then cooled down to room temperature. Fifty milliliters of ethanol was added to the solution and the suspension was centrifuged at 6000 rpm for 30 min. The supernatant was removed and the crude material was washed with solvent several times to remove the unbonded excess ligands. Finally, Au-oley was redispersed in 50 mL of nonpolar heptane to give a red dispersion.

Synthesis of Thiol-Stabilized Au NPs (Au-L6, Au-L10 and Au-L18). A versatile synthetic approach for preparing thiol-stabled Au NPs through interfacial ligand exchange reactions was done between 15 mL of Au-oley dissolved in heptane and 50 μL of thiol ligands with different carbon chain lengths including hexanethiol (Au-L6), decanethiol (Au-L10), and octadecylthiol (Au-L18).[52,53] All the synthetic conditions were similar to the preparation of Au-oley. Upon completion of the exchange, similar purification procedures were used and the obtained final alkylthiol-stabled Au NPs products were soluble/redispersed in heptanes.

Characterization. X-ray photoelectron spectroscopy (XPS) measurements were collected using VG ESCA Scientific Theta Probe spectrometer. The optical measurements were performed with a JASCO V-670 UV-Vis spectrometer. The thickness of polymer hybrid film was determined with a Microfigure Measuring Instrument (Surfcorder ET3000, Kosaka Laboratory Ltd.). Contact-angle measurement were made using CAM 110 (Creating Nano Tech. Inc.). The morphologies of the prepared Au NPs in F8T2 matrix were characterized by the transmission electron microscope (TEM, JEOL 1230) and Nanoscope 3D Controller atomic force micrographs (AFM, Digital Instruments) operated in the tapping mode at room temperature.

Device Fabrication and Measurement. The present OTFTs devices are the bottom-gate and top-contact type configuration and the cross section schematic diagram is shown in Figure 1. The highly doped Si wafer covered by a thermally grown 300-nm-thick silicon dioxide (SiO_2) was used as bottom gate substrate. Subsequently, the Si wafer was immersed in solution of silanes (0.2 mM in decane) for 24 h to form a SAM including n-propyltriethoxysilane (C_3−SAM), n-hexyltriethoxysilane (C_6−SAM), n-octyltriethoxysilane (C_8−SAM), and n-dodecyltriethoxysilane (C_{12}−SAM). Nonreacted silanes were removed by rinsing with decane for several times and the devices were dried under constant nitrogen flow. The hydrophobic qualities of the SAM were verified by contact angle measurements. A layer of F8T2:Au NPs nanocomposites was then deposited on top by spin-coating a polymer hybrid solution in anhydrous xylene at a speed of 2000 rpm for 60 s and immediately annealed at 100 °C for 60 min. Source and drain gold electrodes (80 nm) were thermally evaporated through a shadow mask. All the procedures and measurements were carried out inside a N_2-filled glove box. The electrical characteristics of memory devices were measured in the dark at room temperature using Keithley 4200 semiconductor parameter analyzer. Ten testing cells per OTFT device were characterized to access reproducibility.

RESULTS AND DISCUSSION

Characterization of Ligand-Stabilized Au NPs. Interfacial ligand exchange reaction was used to incorporate functionalities in the ligand shell of thiol-stabilized Au NPs. The natures of the Au NPs were verified by UV-Vis and X-ray photoelectron spectroscopy (XPS) as shown in Figure 1 and

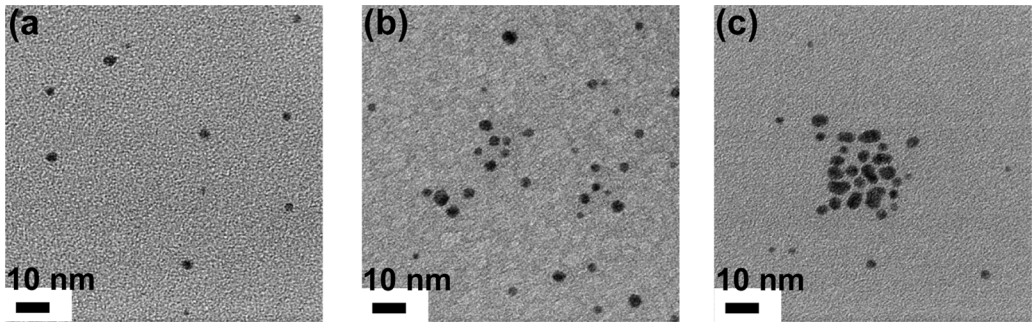

Figure 2. TEM image of F8T2:Au NPs hybrid thin films using different ligand chain lengths: (a) Au-L18, (b) Au-L10, and (c) Au-L6.

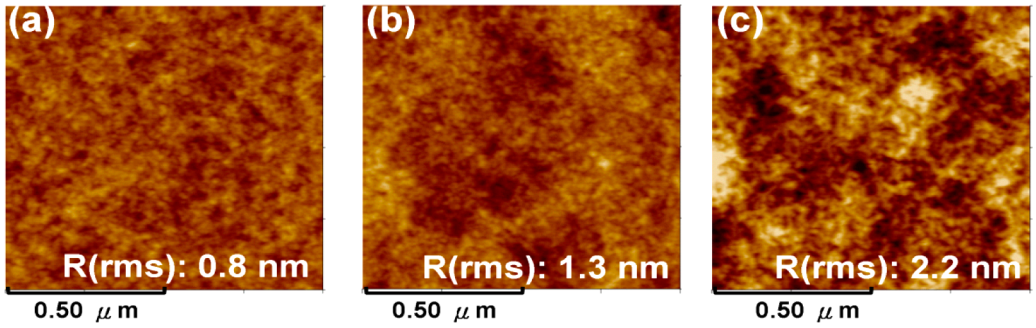

Figure 3. AFM images of F8T2:9% Au NPs hybrid thin films on the C_{12}−SAM modified SiO_2 surface in the case of (a) Au-L18, (b) Au-L10, and (c) Au-L6.

Figure S1 in the Supporting Information. Position and intensity of absorption band are strongly dependent on the size and shape of Au NPs. For the optically functionalized Au NPs with small diameters, the surface plasmon resonance band is found at ∼520 nm in the UV−Vis spectra of thiol-stabilized Au NPs with different lengths of ligand shells in solution (Figure 1).[38,48] In addition, no significant change in solution color (Figure S2 in the Supporting Information) from starting solution indicates that similar NPs size can be preserved even after the exchange reaction. Therefore, the colloidal stability is maintained in our synthesized thiol-capped Au NPs. The thiol-stabilized ligands after purification were experimentally confirmed by the XPS analysis with the absence of N 1s and accompanied presence of S 2p providing the evidence for successful ligands exchange (see Figure S1 in the Supporting Information). The quantitative sizes of the spin-cast hybrid thin films from the solution of 9% Au NPs relative to F8T2 are shown in the TEM graphs (Figure 2). Thiol-capped Au NPs yields uniform diameter of 8.5 ± 1.3 nm. In the high-magnitude TEM image of Figure 2, the Au-L6 apparently undergo "nanoscale aggregation" and parts of their interparticle distances become smaller than a single Au NP, resulting in the broaden absorption peak at a higher wavelength. Au-L6 with less bulky ligands lead to have a close packing in the solid phase. Densities of thiol-stabilized Au NPs in F8T2 matrix estimated from TEM images are 1×10^{-11}, 6×10^{-12}, and 5×10^{-12} cm^{-2} for Au-L6, Au-L10 and Au-L18, respectively. The surface structure of ∼30 nm thick hybrid film of F8T2:Au NPs evaluated by AFM is shown in Figure 3. Whereas F8T2:Au-L18 or Au-L10 film exhibits very flat and smooth surface with a RMS roughness of ∼1 nm, F8T2:Au-L6 nanocomposite thin film exhibits a slightly increasing roughness consistent with the Au NPs diameter measured by TEM. Furthermore, the AFM images of F8T2:Au NPs indicate a random and homogeneous distribution of NPs on the hybrid films for the channel in OTFTs.

Hybrid Nanocomposites OTFT Memory Characteristics. The operation of OTFTs memories depends on the charge trapping/detrapping in the hybrid layer comprising stabilized Au NPs incorporated into semiconducting F8T2. The memory devices are programmed or erased under a dual external voltage sweep. Note that all the measurements were performed in the dark to minimize the possibilities on optical switching effect. First, to investigate the influence of dielectric surface modification on device performance, a strategy has been followed using the SAM of organosilane compounds with different alkyl chain lengths (C_6−SAM, C_8−SAM, and C_{12}−SAM, see Figure S3 in the Supporting Information). Aqueous advancing contact angles increase from 91.1° of the substrates modified with C_3−SAM to 97.5, 108.4, and 110.4° for C_6−SAM, C_8−SAM, and C_{12}−SAM (see Figure S3 in the Supporting Information), respectively. The chemically bound silane moiety provides the hydrophobic surface. Besides, the drain current at high negative gate bias saturates in OTFTs, following the standard p-type semiconducting behavior (see Figure S4 in the Supporting Information). Table S1 in the Supporting Information summarizes the results for mobility, ON/OFF ratio and threshold voltage shift (V_{th}) of nanocomposites OTFTs memory device. The threshold voltage is defined as the intercept of a linear least square fit to $I_d^{1/2}$ versus V_g. The average mobility with standard deviation was calculated from the slope of 5 samples. From the data presented in Table S1 in the Supporting Information, it is clearly that substrates coated with SAM exhibit an improved device performance, achieving an average carrier mobility up to 5.86×10^{-3} cm^2 V^{-1} s^{-1} for C_{12}−SAM (ten times higher compared to SiO_2 dielectric) that is comparable to the devices reported in the literature.[54] SiO_2 dielectric modified with a longer alkylsilane on SAM exhibits a slightly higher mobility than those achieved

with shorter chains on SAM. The ordering in the SAM is probably enhanced as the alky chain length is increased, inducing a more ordering in F8T2 layers.[55] Therefore, all the hybrid OTFTs memory devices discussed later were deposited under the same C_{12}−SAM-modified SiO_2 surface to pursuit the best device characteristics.

The hybrid nanocomposites device performances were studied as a function of (a) the composition (wt %) of Au-oley in the F8T2 film ranging from 0 to 3, 5, 7, and 9% or (b) ligand-capped Au NPs coated with different organic thiolate lengths based on Au-L6, Au-L8, and Au-L18. TEM images show that a relatively good dispersion of Au NPs in the F8T2 thin film, which has a size of 8.5 nm. In addition, Au NPs are gradually distributed more closely as increasing the Au NPs concentration (see Figure S5 in the Supporting Information). Figure 4 shows the transfer characteristics of hybrid devices

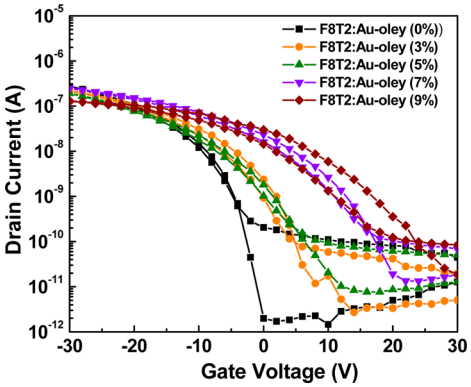

Figure 4. $I_d - V_g$ transfer characteristics at $V_d = -15$ V of F8T2:Au-oley (from 0 to 3, 5, 7, and 9%) hybrid nanocomposite memory device.

with different Au-oley doping concentrations upon double sweeping at drain voltage (V_d) of −15 V. Near-zero threshold voltage shift/almost no hysteresis in the transfer curve in neat F8T2 film (black line; square filled makers) can exclude the intrinsic trap at the bulk domain boundary or interface between organic semiconductor layer and gate dielectric surface. However, OTFTs with F8T2:Au-oley channel layer exhibits the p-type characteristics but transfer curve shows current hysteresis, probably arising from the energy level barrier at F8T2/Au NPs interface. The cyclic sweeping of the V_g was operated from 30 V (programming) to −30 V (erasing) and then back to 30 V (Figure 4) and this hysteresis in transfer curve approaches to be saturated during the applied V_g of ±30 V. After the device turns ON (initially from positive V_g), there is a rapid increase in the I_d with a negative bias in V_g because of the absence of the trapping charges. When the V_g approaches zero, the I_d still remains in the high conductance (programmed) state with a nonvolatile feature. The subsequent application of negative V_g on the device switches off the device (reverse voltage sweep), leading to a decrease in I_d. The nonvolatility based on the accumulation of trapped charges in Au-oley keeps the device in the low conductance (erased) state. The anticlockwise hysteresis loop during the forward (30 V to −30 V) and reverse (-30 V to 30 V) sweeps with a threshold voltage shift in F8T2:Au-oley hybrid device implies that the origin of the memory effect is in relation to the positive charge trapped in the interface controlled by the gate electric field. From these electrical measurements, the essential threshold voltage shift is referred to be the memory window that depends on the Au NPs doping concentration. The F8T2:Au-oley nanocomposites based OTFTs memories show a wide range of memory window starting from 1.44 V to 5.28 V as the Au-oley concentration increases (Figure 4). These results signify that the charge transfer from F8T2 to Au-oley is enhanced with Au-oley concentration as the trapping sites. Similar trends on the threshold voltage shift in $I_d - V_g$ studies were detected on C_3−SAM, C_6−SAM, and C_8−SAM-modified dielectric and summarized the performance of all measured F8T2:Au-oley devices at Table S1 in the Supporting Information.

It has been reported that the change in threshold voltage may be from the result of the macroscopic dipole moment of the SAM.[56] However, nonpolar alkylsilane groups indicate the zero surface potential on the SAM dielectric without charge trapping ability. No significant difference in the memory window is observed for a fixed Au-oley concentration using the different SAM modified SiO_2 dielectric. Therefore, the observed hysteresis is mainly attributed to the charge trapping effect from the Au-oley embedded in the F8T2 matrix. From Table S1 in the Supporting Information, the mean charge carrier mobility values extracted from the saturation region are in a reverse trend with the Au-oley concentration. It shows the largest mobility for bare F8T2 and the lowest for 9% Au-oley in F8T2 for all SAM-modified dielectrics because of the disruption of $\pi-\pi$ conjugation of F8T2 stacked architecture by the Au NPs. However, the hybrid device fabricated at C_{12}−SAM dielectric reveals a slightly improved mobility (but still in the same order of magnitude) among all the SAM-modified surfaces, using the same concentration of Au-oley. The efficient intermolecular $\pi-\pi$ overlapping in the solid state intensified by more hydrophobic surface can promote charge transport properties, characterized by broader absorption range in the UV−Vis spectrum of F8T2 thin film at C_{12}−SAM dielectric (see Figure S6 in the Supporting Information).

From the above discussions, we optimized the suitable concentration (∼9 %) of Au NPs in OTFTs on the C_{12}−SAM modified SiO_2 surface to ensure the clear electrical margin within a saturated/critical state. Stable Au-oley undergo interfacial ligand exchange method to produce Au NPs decorated with different alkylthiolated chain lengths of 6 (Au-L6), 10 (Au-L10), and 18 (Au-L18). Therefore, the electrical characteristics of OTFTs using the hybrid materials of F8T2:Au-L6 or Au-L10 or Au-L18 are shown in Figure 5a. All the transfer curves of the hybrid devices show the typical current modulation characteristics of p-type active layers at a forward sweep from 30 V to −30 V. When the device is swept backward to 30 V, anticlockwise current hysteresis is observed with a memory window, defined as the threshold voltage shift between two sweeps, of approximately 5 ± 4, 9 ± 2, and 41 ± 4 V for devices based on Au-L18, Au-10, and Au-L6, respectively, larger for the ligand-capped NPs with a shorter alkylthiolated length. The negative threshold voltage shift in the cyclic sweeps is reversible and it is assigned to be the data retrieval of memory storage device. Larger memory window means that the existence of Au-L6 has an enhanced charge capturing ability. In addition, the devices exhibit the field effect mobilities of $(1.83 \pm 0.33) \times 10^{-3}$, $(8.31 \pm 0.28) \times 10^{-4}$, and $(5.54 \pm 0.25) \times 10^{-4}$ cm^2 V^{-1} s^{-1} for Au-L18, Au-L10, and Au-L6, respectively, at the V_d of −15 V with an ON/OFF ratio of $\sim 1 \times 10^4$ based on transistor operation current. The OTFTs devices behave as bistable memories and at V_g of 0 V the current in the programmed and erased state differs by more

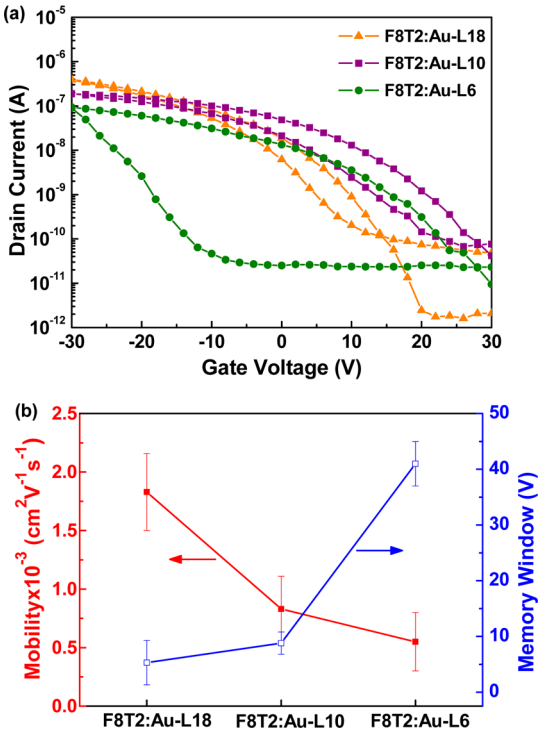

Figure 5. (a) $I_d - V_g$ transfer characteristics at $V_d = -15$ V of OTFTs memory devices using the hybrid nanocomposites of F8T2:Au NPs (Au-L18 or Au-L10 or Au-L6). (b) Mobility and memory window of hybrid materials based OTFTs memory device as a function of chain length of alkylthiol-capped on Au NPs.

than three orders of magnitudes (memory ratio $>1 \times 10^3$) for the F8T2:Au-L6 device. As noted, the memory window increases and mobility decreases continuously with a decrease in the alkylthiolate chain length (Figure 5b). The resultant increase in total density of the stored charges, Δn, in Au NPs with different ligands can be approximately estimated from the relation[22]

$$\Delta n = \frac{\Delta V_{th} C_i}{e} \quad (1)$$

where e is the element charge and C_i is the unit area capacitance for SiO_2 dielectric. By comparing the stored charge density from eq 1 and the average area density of Au NPs, Δn are 4.5×10^{12}, 5.4×10^{11}, and 8.7×10^{11} cm^{-2} within Au-L6, Au-L10, and Au-L18, embedded in the F8T2, respectively, i.e., about 45, 5, 2 average trapped charges per Au NP in the hybrid device. It can be noticed that the charge storage capacity increases after Au NPs functionalized with a shorter alkylthiolate length, indicating that the ligand size on Au NPs plays an important role in charge transport and trap environment.

We also investigated the static and dynamic charge retention behaviors of the hybrid transistor memories, i.e., the relaxation dynamics of trapped charge carriers between the programmed and erased states. To judge the nonvolatility of the programmable memory device based on F8T2:Au-L6 hybrid thin film, statistic retention measurements as a function of time were analyzed after applying 30 V or −30 V V_g bias for 1 s to the device in order to generate the programmed or erased state, respectively (Figure 6). The device retention time is defined as the time duration of the charge storage in the Au NPs without any current leakages. Figure 6 shows plots on I_d vs time of F8T2:9% Au-L6 hybrid device with the C_{12}−SAM-modified

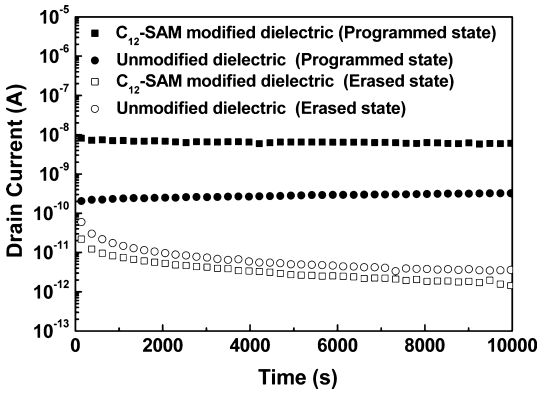

Figure 6. Retention time test for F8T2:9% Au-L6 hybrid materials based OTFTs memory devices on the bare SiO_2 surface or C_{12}−SAM-modified SiO_2 surface.

(square symbols) or unmodified dielectric (circle symbols) for the programmed (solid symbols) and erased (open symbols) state measured at a time interval of 10 s at $V_g = 0$ V and $V_d = -15$ V. A considerable programmed state/erased state current ratio of $>1 \times 10^3$ in the hybrid device is maintained for at least 1×10^4 s, but both the drain currents slightly decrease with time. Our hybrid memory device has a comparable difference in current states relative to the general nonvolatile floating gate using Au NPs sandwiched between tunneling/blocking layers.[20−29] However, relatively rapid dissipation/relaxation of trapped charges occurs in hybrid device without the SAM-modified dielectric originally from parasitized structural defects or impurities near the dielectric/semiconductor interface, implying that the charge storage strategy from direct hybrids of organic semiconductor and Au NPs needs to be more emphasized for further featuring the device characteristics. Additionally, the dynamic response of F8T2:Au-L6 hybrid nanocomposites OTFTs memories was also measured. The dynamic input signal with programming (30 V) and erasing (−30 V) was applied and dynamic current response was recorded between them (reading at 0 V_g), as shown in the repetitive cycles of Figure 7(a). Hybrid nanocomposites memories operated in this way show reversible and stable switching behaviors between the programmed and erased states with a conductance change of $\sim 1 \times 10^3$ being constantly maintained for at least 100 cycles (Figure 7b). The sustainable retention capabilities indicate that the as-fabricated F8T2:ligand-capped Au NPs hybrid nanocomposites memories can function as good candidate for stable nonvolatile memory device.

Switching Mechanism. The switching mechanism for memory effect is further suggested as the following. The role of the charging/discharging mechanism of gate bias-induced charge carriers should be emphasized, recording the forward/reverse cycles at a specific voltage range.[57] Because the F8T2 transistors operate in the p-channel accumulation, the major carrier is hole. The presence of Au NPs affects the overall charge distribution in the current channel. It is sure that the hole trapping in the Au NPs charge storage sites rather than polarization or defect in gate dielectric dominates the electrical hysteresis because of the negligible hysteresis loop of pure F8T2-based OTFTs device (without Au NPs) (Figure 4). NP-based devices show the memory effect due to the charge storage capability. However, NPs aggregation within the F8T2 matrix may disrupt the long-range ordering structures but

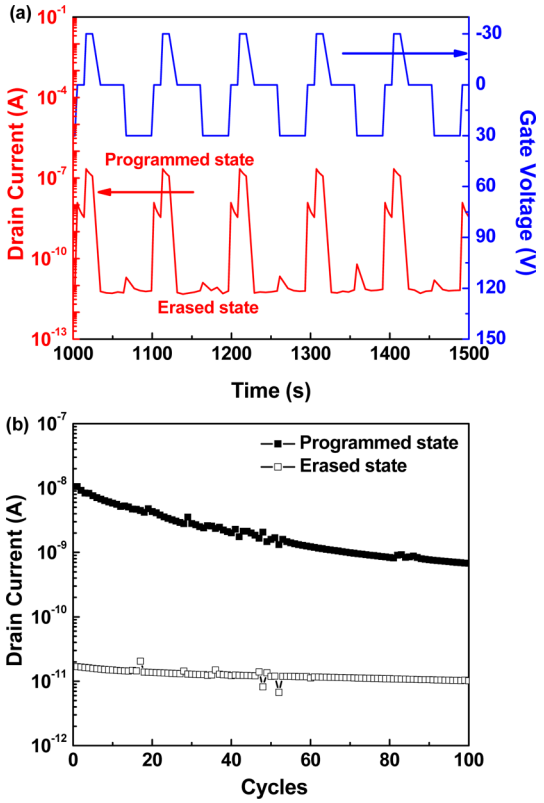

Figure 7. (a) Reversible and reproducible switching between programmed/erased states and (b) Endurance characteristics of F8T2:9% Au-L6 hybrid OTFTs memory devices.

increase the charge retention effect. Also, different ligand-coating with a given concentration of NPs gives the tunneling barrier for the positive charge to reach the NPs core. When the V_g scans from positive bias to negative bias (over the V_{th}), the device starts from the exhaust region to the hole accumulation in the channel and the traps in the channel are charged gradually. At this sweep, the I_d increases with the negative V_g and more holes can be captured in the Au NPs. As a result, the internal electric field generated by these trapped charges modulates the channel conductance together with the applied gate voltage and the increase in I_d becomes saturated until the traps are fully filled. However, the opposite field between internal electric filed and applied bias causes the important screening effect. As the V_g returns back to the positive value, the trapped holes in Au NPs gradually releases to attend conductance and trapped holes still offset the channel conductance, resulting in a lower I_d from free charge with respect to the case of V_g scanned from the positive to negative value (at the same V_g condition).[34−37] Therefore, higher concentration of F8T2:Au-oley hybrid device can feature a reduced mobility and larger memory window for charge storage.

Furthermore, for the OTFTs memories with same processing condition and device architecture but difference in the ligands for capping the Au NPs, the memory window and field-effect mobility show significant difference. Alkylthiol ligands can disperse the Au NPs well in F8T2. Among them, the greatest negative threshold voltage shift is observed in the Au-L6-based hybrid device determined by the surface potential of functionalized Au NP surface,[34] so that the holes in the semiconducting channel have chances of being transferred to the Au NPs through F−N tunneling and being captured. The reduction of tunneling barrier between F8T2 and Au NPs after surface modification based on shorter chain of alkylthiol ligand facilitates the holes to inject into the Au NPs.[34] Therefore, the ligand in shorter chain length (in other words, thinner ligands on Au NPs) leads to a low contribution of tunneling resistance to the charge trapping process, resulting in the larger memory window.

To determine the response of the charge trapping on the electrical hysteresis characteristics, subsequent I_d−V_g measurements of 9% Au-L6 hybrid nanocomposites devices were taken under the dual sweep from 5 V to various specific sweeping V_g ($V_{g(sweep)}$) (in negative value) as shown in Figure 8a, and

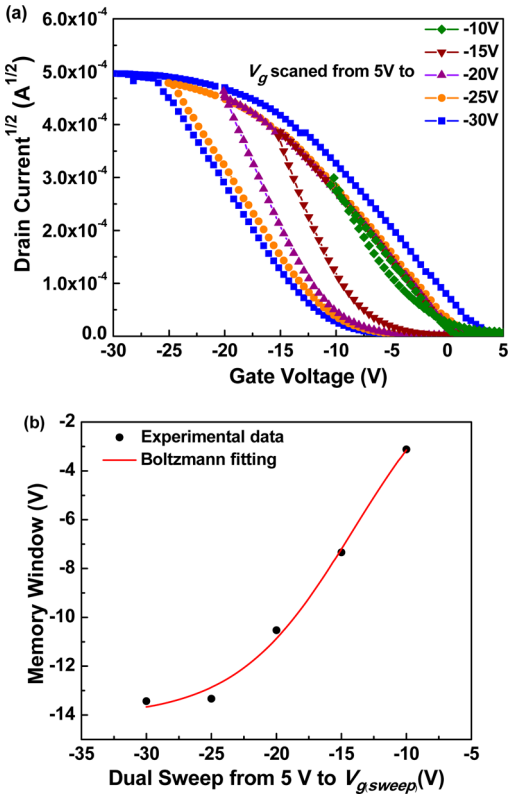

Figure 8. (a) Memory window of the F8T2:9% Au-L6 hybrid materials based OTFTs memory devices under the dual sweep from 5 V to various $V_{g(sweep)}$. (b) Statistical analysis between memory window and dual sweep from 5 V to $V_{g(sweep)}$.

corresponding memory window obtained from 5 V to $V_{g(sweep)}$ were analyzed (Figure 8b). There is a small distinguishable threshold voltage shift when the $V_{g(sweep)}$ equals −10 V. As $V_{g(sweep)}$ is incrementally enhanced, the threshold voltage in the back sweep moves to a more negative direction and memory window increases up to saturation near critical $V_{g(sweep)}$ = −25 V that is entirely demonstrated by the Boltzmann fitting. These results support that our direct hybrid materials as a channel for OTFTs memories retain the information storage (as high as ∼41 V memory window) with the low power consumption (within ±30 V), whereas other conditions keep similar (300 nm thick SiO_2 dielectric/Si substrate and device geometries) as compared to the previous reported NPs-containing floating gate device as additional charge storage hybrid layer.[30−33] For example, uniform metal NPs can be fabricated within block copolymer template,[30−33] but higher operation voltage (at least

±60 V)[32,33] and metal NPs loading concentration (at least 40%)[33] needs to overcome to reach similar (or worse) memory performance due to the power consumption between the charge storage/semiconducting double layers. Further approach to reduce the operation voltages in our study is to enhance the gate dielectric capacitance though a reduced SiO_2 dielectric or high dielectric constant gate dielectric; however, current leakage should be more considered to balance all issues.

CONCLUSIONS

We have successfully realized the nanocomposites OTFTs memory by blending inorganic Au NPs within semiconducting F8T2 polymer layer as storage site when the Au NPs are functionalized with different alkylthiols lengths. Counterclockwise hysteresis loop in the I_d−V_g curve was observed with increasing gate sweeping ranges due to the memory effect from trapped holes within the Au NPs. The concentration and organic ligands attachments of Au NPs play a crucial role in the efficiency of charge trapping/detrapping process, implying that the charge tunneling barriers can determine the hole storage with tunable memory windows. Additionally, this direct hybrid method can obtain good memory performances such as large enough memory windows and low operation voltages and be potentially integrated with other organic electric components.

ASSOCIATED CONTENT

Supporting Information

Additional electrical characteristics of Au NPs hybrid nanocomposite memory device. XPS spectra and solution in heptane of Au-L6, Au-L10, and Au-L18. Contact angle measurements of C_3−SAM, C_6−SAM, C_8−SAM and C_{12}−SAM modification on SiO_2 substrate. I_d−V_d curve for F8T2:9% Au-oley hybrid nanocomposites memory devices for different SAM-modified SiO_2 dielectrics. TEM image and Optical absorption spectra of F8T2:Au-oley thin films. This material is available free of charge via the Internet at http://pubs.acs.org/.

AUTHOR INFORMATION

Corresponding Authors

*E-mail: chenwc@ntu.edu.tw.
*E-mail: clliu@ncu.edu.tw.

Notes

The authors declare no competing financial interest.

ACKNOWLEDGMENTS

The authors acknowledge final support from National Science Council of Taiwan.

REFERENCES

(1) Arias, A. C.; MacKenzie, J. D.; McCulloch, I.; Rivnay, J.; Salleo, A. *Chem. Rev.* **2010**, *110*, 3−24.
(2) Sokolov, A. N.; Tee, B. C. K.; Bettinger, C. J.; Tok, J. B. H.; Bao, Z. *Acc. Chem. Res.* **2011**, *45*, 361−371.
(3) Sekitani, T.; Someya, T. *Adv. Mater.* **2010**, *22*, 2228−2246.
(4) Guo, Y.; Yu, G.; Liu, Y. *Adv. Mater.* **2010**, *22*, 4427−4447.
(5) Di, C.-a.; Zhang, F.; Zhu, D. *Adv. Mater.* **2013**, *25*, 313−330.
(6) Ling, Q.-D.; Liaw, D.-J.; Zhu, C.; Chan, D. S.-H.; Kang, E.-T.; Neoh, K.-G. *Prog. Polym. Sci.* **2008**, *33*, 917−978.
(7) Dhar, B. M.; Özgün, R.; Dawidczyk, T.; Andreou, A.; Katz, H. E. *Mater. Sci. Eng., R* **2011**, *72*, 49−80.
(8) Heremans, P.; Gelinck, G. H.; Müller, R.; Baeg, K.-J.; Kim, D.-Y.; Noh, Y.-Y. *Chem. Mater.* **2010**, *23*, 341−358.
(9) Leong, W. L.; Mathews, N.; Tan, B.; Vaidyanathan, S.; Dotz, F.; Mhaisalkar, S. *J. Mater. Chem.* **2011**, *21*, 5203−5214.
(10) Lee, J.-S. *J. Mater. Chem.* **2011**, *21*, 14097−14112.
(11) Naber, R. C. G.; Asadi, K.; Blom, P. W. M.; de Leeuw, D. M.; de Boer, B. *Adv. Mater.* **2010**, *22*, 933−945.
(12) Baeg, K. J.; Noh, Y. Y.; Ghim, J.; Kang, S. J.; Lee, H.; Kim, D. Y. *Adv. Mater.* **2006**, *18*, 3179−3183.
(13) Huang, C.; West, J. E.; Katz, H. E. *Adv. Funct. Mater.* **2007**, *17*, 142−153.
(14) Baeg, K.-J.; Noh, Y.-Y.; Ghim, J.; Lim, B.; Kim, D.-Y. *Adv. Funct. Mater.* **2008**, *18*, 3678−3685.
(15) Guo, Y.; Di, C.-a.; Ye, S.; Sun, X.; Zheng, J.; Wen, Y.; Wu, W.; Yu, G.; Liu, Y. *Adv. Mater.* **2009**, *21*, 1954−1959.
(16) Hsu, J.-C.; Lee, W.-Y.; Wu, H.-C.; Sugiyama, K.; Hirao, A.; Chen, W.-C. *J. Mater. Chem.* **2012**, *22*, 5820−5827.
(17) Chou, Y.-H.; You, N.-H.; Kurosawa, T.; Lee, W.-Y.; Higashihara, T.; Ueda, M.; Chen, W.-C. *Macromolecules* **2012**, *45*, 6946−6956.
(18) Chiu, Y.-C.; Liu, C.-L.; Lee, W.-Y.; Chen, Y.; Kakuchi, T.; Chen, W.-C. *NPG Asia Mater.* **2013**, *5*, e35.
(19) Chou, Y.-H.; Yen, H.-J.; Tsai, C.-L.; Lee, W.-Y.; Liou, G.-S.; Chen, W.-C. *J. Mater. Chem. C* **2013**, *1*, 3235−3243.
(20) Zhengchun, L.; Fengliang, X.; Yi, S.; Lvov, Y. M.; Varahramyan, K. *IEEE Trans. Nanotechnol.* **2006**, *5*, 379−384.
(21) Kim, S.-J.; Song, J.-M.; Lee, J.-S. *J. Mater. Chem.* **2011**, *21*, 14516−14522.
(22) Baeg, K.-J.; Noh, Y.-Y.; Sirringhaus, H.; Kim, D.-Y. *Adv. Funct. Mater.* **2010**, *20*, 224−230.
(23) Han, S.-T.; Zhou, Y.; Xu, Z.-X.; Huang, L.-B.; Yang, X.-B.; Roy, V. A. L. *Adv. Mater.* **2012**, *24*, 3556−3561.
(24) She, X.-J.; Liu, C.-H.; Zhang, J.-Y.; Gao, X.; Wang, S.-D. *Appl. Phys. Lett.* **2013**, *102*, 053303−5.
(25) Han, S.-T.; Zhou, Y.; Wang, C.; He, L.; Zhang, W.; Roy, V. A. L. *Adv. Mater.* **2013**, *25*, 793−793.
(26) Han, S.-T.; Zhou, Y.; Xu, Z.-X.; Roy, V. A. L.; Hung, T. F. *J. Mater. Chem.* **2011**, *21*, 14575−14580.
(27) She, X.-J.; Liu, C.-H.; Sun, Q.-J.; Gao, X.; Wang, S.-D. *Org. Electron.* **2012**, *13*, 1908−1915.
(28) Chang, H.-C.; Lee, W.-Y.; Tai, Y.; Wu, K.-W.; Chen, W.-C. *Nanoscale* **2012**, *4*, 6629−6636.
(29) Kang, M.; Baeg, K.-J.; Khim, D.; Noh, Y.-Y.; Kim, D.-Y. *Adv. Funct. Mater.* **2013**, *23*, 3482−3482.
(30) Leong, W. L.; Mathews, N.; Mhaisalkar, S.; Lam, Y. M.; Chen, T.; Lee, P. S. *J. Mater. Chem.* **2009**, *19*, 7354−7361.
(31) Leong, W. L.; Mathews, N.; Tan, B.; Vaidyanathan, S.; Dotz, F.; Mhaisalkar, S. *J. Mater. Chem.* **2011**, *21*, 8971−8974.
(32) Chen, C.-M.; Liu, C.-M.; Wei, K.-H.; Jeng, U. S.; Su, C.-H. *J. Mater. Chem.* **2012**, *22*, 454−461.
(33) Wei, Q.; Lin, Y.; Anderson, E. R.; Briseno, A. L.; Gido, S. P.; Watkins, J. J. *ACS Nano* **2012**, *6*, 1188−1194.
(34) Tseng, C.-W.; Tao, Y.-T. *J. Am. Chem. Soc.* **2009**, *131*, 12441−12450.
(35) Zhou, Y.; Han, S.-T.; Xu, Z.-X.; Roy, V. A. L. *Adv. Mater.* **2012**, *24*, 1247−1251.
(36) Wang, S.; Leung, C.-W.; Chan, P. K. L. *Org. Electron.* **2010**, *11*, 990−995.
(37) Wang, S.; Chan, P. K. L.; Wah Leung, C.; Zhao, X. *RSC Adv.* **2012**, *2*, 9100−9105.
(38) Han, S.-T.; Zhou, Y.; Xu, Z.-X.; Roy, V. A. L. *Appl. Phys. Lett.* **2012**, *101*, 033306−5.
(39) Liu, G.; Ling, Q.-D.; Teo, E. Y. H.; Zhu, C.-X.; Chan, D. S.-H.; Neoh, K.-G.; Kang, E.-T. *ACS Nano* **2009**, *3*, 1929−1937.
(40) Liu, J.; Lin, Z.; Liu, T.; Yin, Z.; Zhou, X.; Chen, S.; Xie, L.; Boey, F.; Zhang, H.; Huang, W. *Small* **2010**, *6*, 1536−1542.
(41) Islam, M. M.; Pola, S.; Tao, Y.-T. *ACS Appl. Mater. Interfaces* **2011**, *3*, 2136−2141.
(42) Liu, J.; Zeng, Z.; Cao, X.; Lu, G.; Wang, L.-H.; Fan, Q.-L.; Huang, W.; Zhang, H. *Small* **2012**, *8*, 3517−3522.
(43) Kim, T. W.; Yang, Y.; Li, F.; Kwan, W. L. *NPG Asia Mater* **2012**, *4*, e18.

(44) Yu, A.-D.; Liu, C.-L.; Chen, W.-C. *Chem. Commun.* **2012**, *48*, 383−385.
(45) Chen, J.-C.; Liu, C.-L.; Sun, Y.-S.; Tung, S.-H.; Chen, W.-C. *Soft Matter* **2012**, *8*, 526−535.
(46) Tseng, C.-W.; Huang, D.-C.; Tao, Y.-T. *ACS Appl. Mater. Interfaces* **2012**, *4*, 5483−5491.
(47) Tseng, C.-W.; Huang, D.-C.; Tao, Y.-T. *ACS Appl. Mater. Interfaces* **2013**, *4*, 9528−9536.
(48) Liu, C.-L.; Chen, W.-C. *Polym. Chem.* **2011**, *23*, 2169−2174.
(49) Aleshin, A. N.; Alexandrova, E. L. 2008, *50*, 1895-1900.
(50) Yu, A.-D.; Kurosawa, T.; Chou, Y.-H.; Aoyagi, K.; Shoji, Y.; Higashihara, T.; Ueda, M.; Liu, C.-L.; Chen, W.-C. *ACS Appl. Mater. Interfaces* **2013**, *4*, 4921−9536.
(51) Chang, H.-C.; Liu, C.-L.; Chen, W.-C. *Adv. Funct. Mater.* **2013**, *23*, 4960−4968.
(52) Warner, M. G.; Reed, S. M.; Hutchison, J. E. *Chem. Mater.* **2000**, *12*, 3316−3320.
(53) Shen, C.; Hui, C.; Yang, T.; Xiao, C.; Tian, J.; Bao, L.; Chen, S.; Ding, H.; Gao, H. *Chem. Mater.* **2008**, *20*, 6939−6944.
(54) Lim, E.; Jung, B.-J.; Chikamatsu, M.; Azumi, R.; Yoshida, Y.; Yase, K.; Do, L.-M.; Shim, H.-K. *J. Mater. Chem.* **2007**, *17*, 1416−1420.
(55) Jedaa, A.; Burkhardt, M.; Zschieschang, U.; Klauk, H.; Habich, D.; Schmid, G.; Halik, M. *Org. Electron.* **2009**, *10*, 1442−1447.
(56) Gholamrezaie, F.; Andringa, A.-M.; Roelofs, W. S. C.; Neuhold, A.; Kemerink, M.; Blom, P. W. M.; de Leeuw, D. M. *Small* **2012**, *8*, 241−245.
(57) Egginger, M.; Bauer, S.; Schwödiauer, R.; Neugebauer, H.; Sariciftci, N. *Monatsh Chem.* **2009**, *140*, 735−750.